# Development of a new method to estimate the incident solar flux on central receivers from deteriorated heliostats

M.R. Rodríguez-Sánchez, C. Leray, Adrien Toutant, A. Ferriere, G. Olalde

Renewable Energy 130 (2019) 182–190

Contents lists available at ScienceDirect

Renewable Energy

journal homepage: www.elsevier.com/locate/renene

# Development of a new method to estimate the incident solar flux on central receivers from deteriorated heliostats

M.R. Rodríguez-Sánchez [a, *], C. Leray [b], A. Toutant [b, c], A. Ferriere [b], G. Olalde [b]

[a] Energy Systems Engineering Group (ISE), Department of Fluids and Thermal Engineering, Universidad Carlos III of Madrid, Av. Universidad 30, Leganés, 28911, Madrid, Spain
[b] Laboratoire PROcédés, Matériaux, Energie Solaire (PROMES), UPR 8521 CNRS, 7 rue du Four Solaire, 66120 Odeillo, France
[c] Université de Perpignan, Via Domitia, 52 avenue Paul Alduy, 66860 Perpignan Cedex 9, France

ARTICLE INFO

*Article history:*
Received 9 March 2018
Received in revised form
13 June 2018
Accepted 14 June 2018
Available online 18 June 2018

*Keywords:*
Solar power tower
Heliostat
Incident solar flux
Digital image analysis

ABSTRACT

This work proposes a new empirical direct methodology to estimate both the solar flux distribution and intensity on the surface of central receivers. In solar power tower plants with deteriorated heliostats, the numerical simulations to estimate the incident solar flux are not precise. Hence the thermal behaviour of the receivers cannot be determined. In those cases, direct measurement or semi-empirical methodologies are required to characterize the radiant power on the receiver.

The new methodology proposed, named *"Superposition method"*, consists in the hourly characterization of the reflected solar beam of each individual heliostat by means of a pyrheliometer, a passive screen, a flux sensor, a camera and digital image analysis. According to the aiming strategy used during receiver operation, each individual solar flux distribution and intensity can be gathered to obtain the total incident radiant power on the solar receiver. This non-real-time method has the advantage of reproducing any solar flux distribution on the receiver at present and past time.



## 1. Introduction

Concentrated Solar Power (CSP) is one of the most promising clean energy technologies in the modern society. While solar energy offers the highest renewable energy potential to our planet, CSP can provide dispatchable power in a technically and economically viable way by means of thermal energy storage and/or hybridization [1]. However, the knowledge of this kind of plant has to be improved to operate them in a safely way.

One of the main problems of this kind of plants is associated with the measurement of the incident radiant power on the receiver, without perturbing the power plant operation. The accurate evaluation of the incident solar flux is very important to manage the plant and to determine its performance. If the radiant power per unit area is not high enough the thermal load capacity decreases and the cost of the electricity increases; while if the radiant power per unit area is too high or is bad distributed it can damage the receiver.

Numerous numerical tools have been developed to estimate the incident solar flux during the receiver operation [2]. They can be divided into two main categories [3]: Montecarlo Ray Tracing and convolution methods. The first one consists in a statistical approach that traces a bundle of random rays from the sun, and it is characterized by a high computational cost. Codes as MIRVAL [4], SolTrace [5], Tonatiuh [6], Stral [7] and Solfast [8] belong to this category. The second category is an approximation methodology based on mathematical superposition and convolution of error cones, characterized by a low computational cost, being some of the most popular codes HFLCAL [9], DELSOL3 [10], UNIZAR and CAMPO [11,12], SPTflux [13], PSO [14] and ParHel [15].

Previous methodologies can be deficient when the heliostats are not well aligned, when they are imperfect or when some of their parameters are unknown. In these cases the validation of numerical models is a crucial step [16]. Several are the authors that have used experimental methodologies to validate the results of their numerical simulations: either by correcting the reflectivity of the heliostats [17], the tracking errors [18,19]; or the canting errors [20]. When validation of numerical models is not possible, it is preferable to use experimental methodologies. Röger et al. [21] classified the limited experimental methodologies in 5 groups, which has been summarized in Table 1:

* Corresponding author.
*E-mail address:* mrrsanch@ing.uc3m.es (M.R. Rodríguez-Sánchez).

https://doi.org/10.1016/j.renene.2018.06.056
0960-1481/

i) Indirect methods that use a white diffuse moving bar target placed in front of the receiver surface and a digital camera that record the flux brightness distribution, which is calibrated with a radiometer. This measurement principle was used since the end of the 1970s worldwide in different central receiver projects, e.g., Beam Characterization System (BCS) of Sandia [22], Flux Analysing System of EIR [23], heliostat and receiver measurement system (HERMES I + II, ProHERMES) of the German Aerospace Center (DLR) [24], and CSIRO [25]. This method is able to characterize the flux distribution of all the heliostats aiming the receiver at once. Being its main issue the degradation of the radiometer painting.

ii) Direct methods based on the previous procedure that use flux sensors mounting in the moving bar. MDF method [26] was the most renowned system of this type, which reported an accuracy of about 6%. However, it still had problems with the overheating and the degradation of the white Lambertian surface of the moving bar.

iii) Indirect methods that utilize a digital camera directly on the receiver surface. In this case, the intensities reflected by the images at the receiver surface are calibrated to obtain the incident solar flux on the receiver. The most popular method, named PHLUX method, was employed by Ho and Khalsa [27]. The uncertainties of this method are significantly, up to 20–40%.

iv) Indirect methods that use a stationary stripe-shaped target and sweeping the focus over a fixed target located close to the receiver. The stripe-shaped images, collected with a digital camera, are then merged to gain a composite flux image. Pacheco et al. [28] applied this method by splitting up the heliostats in groups, instead of moving the whole focus at once. Depending on the accuracy of the heliostat tracking, the number of heliostats involved, the spatial shift and the time gap the uncertainty of the flux density distribution reached was in the range from 3.6% to 9.1%.

v) The last direct methods consist in distribute stationary water cooled flux gauges in the aperture plane or on the receiver surface. The problem of this methodology is the moderate spatial resolution and the short lifetime of the flux gauges on high temperature receiver zones, limited to 6 months.

The issue is that nowadays, none of these procedures have been introduced in commercial power plants, since they are not fully developed to measure the solar flux distribution intercepted by the huge receiver surface area with an acceptable spatial resolution. Note also that indirect methods need hypothesis to carry out the estimation of the solar flux distributions that can introduce further uncertainties. For example, the Power-On method proposed by Pacheco [29] to calculate the total incident power on the receiver neglects the influence of the power load in the heat losses, while PROHERMES [24] and MDF [26] estimates the solar flux distribution on the aperture of the cavity, assuming that it is equal to the flux distribution on the receiver surface.

The main goal of this work is to develop an empirical direct methodology to estimate the incident radiant power per unit area on a solar absorber. The experimental method proposed, named "*Superposition method*", lies in the application of the superposition method on luminosity images of the reflected beam of the heliostats, using digital image analysis (DIA) and the measurement of a punctual flux sensor. Although this procedure is well known in numerical procedures, it has not been applied experimentally.

The method proposed can be considered a combination of the fourth and second methods described previously with several updates. The main novelty introduced is that it is a non-real-time method thanks to the creation of an hourly library of the different heliostats. Which is independent of the DNI and the day, using as storage variables the solar time and the concentration ratio. With this library, any combination of the available images can be used to reproduce a solar flux distribution on the receiver at present and past time.

This method could be applied when the numerical simulations are not able to accurately predict the incident radiant power due to the heliostat detriment. This study starts with a description of the plant and the receiver prototype in which it is applied. Secondly, the methodology developed for the estimation of the radiant power on the receiver has been explained. Finally, this new methodology has been verified and validated with several experiments carried out in Themis solar power tower.

## 2. Themis power plant

To carry out this study a prototype solar absorber assembled in Themis solar power tower has been characterized. Themis solar plant consists of a northern solar field layout compound of 107 heliostats, see Fig. 1a. Each heliostat has an effective surface of 53.70 $m^2$ composed of 9 spherical mirror elements installed onto a parabolic supporting structure: eight main modules of 3.62 m × 1.794 m and one central module of 2.46 m × 0.828 m, see Fig. 1b. Each module is individually oriented such as its axis matches the normal to the parabola. In practice, all the modules of each heliostat possess the same focal length, which is close to the

**Table 1**
Summary of the experimental methods to characterize the flux distribution on the receiver surface described in the literature.

| Method | Acquisition devices | Strength | Weakness | Example |
|---|---|---|---|---|
| I Indirect | Diffuse moving bar target<br>Digital camera | High spatial resolution<br>Short measurement time | Radiometer and target degradation | BCS<br>EIR<br>HERMES |
| | Radiometer | High reliability | Mechanical problems of the target | FATMES<br>OBELIX |
| II Direct | Diffuse moving bar target<br>Digital camera<br>Gardon flux gauges | Good spatial resolution<br>Low interpolation errors<br>Better precision than method I (~6%) | Overheating<br>Target degradation<br>No applicable in external receivers | MDF |
| III Indirect | Digital cameras<br>Receiver surface | Simply<br>Cheap | High uncertainties ~20–40%<br>Spectral dependence of the receiver | PHLUX |
| IV Indirect | Stripe-shaped target close to the receiver<br>Digital camera<br>Flux sensor | No mechanical parts | Time gap between heliostats characterization<br>Accuracy function of the number of heliostats | – |
| V Direct | Flux gauges<br>Cooling system | No moving parts<br>Low uncertainties | Low spatial resolution<br>High cost<br>Short gauges lifetime (~6 months) | – |

distance to the receiver aperture. The size, the curvature, the position and the orientation of these facets and the focal length of the supporting structure are known from the design specifications of each individual heliostat, whose initial error ranging was comprised between 0.5 and 2 mrad [30]. Then, the control of the heliostat field should provide the desired intensity and solar flux distribution at the focal volume. However, over the years the heliostats have been deteriorated and some of their facets are missed or broken, therefore nowadays they do not fulfil their initial specifications.

Themis tower is 100 m height and it is equipped with several experimental areas [32]. The receiver prototype consists of a silicon carbide high temperature absorber plate of 1200 mm length, 167 mm width and 28 mm of total thickness [33]. The plate is located at the back wall of a parallelepiped cavity inclined 35.9° with respect to the vertical axis. The cavity has a square aperture area of 1.2 m length and its depth is 1 m. The four lateral walls work as medium temperature absorbers, which preheats the pressurized air that feeds the receiver. The air enters in the high temperature absorber by the right side and exits by the left (see Fig. 2). As the high temperature absorber is small, to avoid overheating only 11 of the 107 heliostats in the field have been used, they have been highlighted in yellow in Fig. 1a.

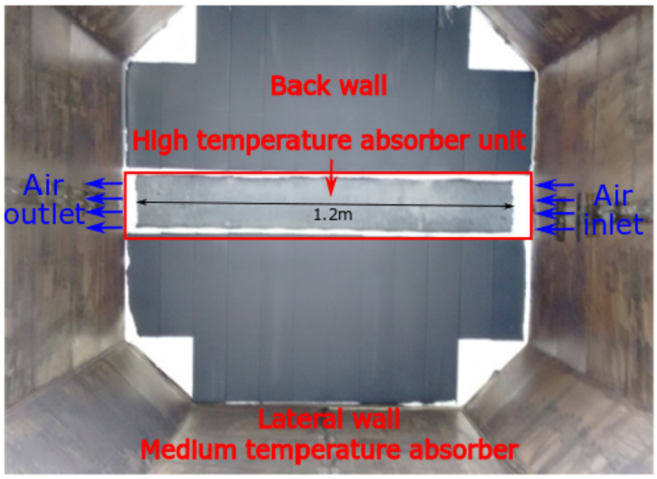


**Fig. 2.** Overview of a ceramic cavity receiver prototype developed by PROMES laboratory installed in Themis.

## 3. Superposition method

Experimentations on the prototype receiver were carried out at Themis from April 2015 to May 2016. In those experiments different operational conditions were tested. A mass flowmeter and several thermocouples allowed to calculate the heat power absorbed by the heat transfer fluid. The estimated incident flux on the receiver, by means of a modified HFCAL simulation [33], resulted to be so high, giving a derisory thermal efficiency of the receiver that did not agree with the numerical study. Therefore, a new methodology to estimate the incident radiant power per unit area is required.

A new experimental methodology named "Superposition method" has been developed to determine the incident solar flux on the receiver surface for any hour, day and aiming strategy. The methodology proposed consists in two main phases. In the first phase, images of the reflected beam of each individual heliostat have been taken and processed to obtain the concentration ratio distribution of each heliostat on the receiver surface. In this first phase, a library of images and concentration ratio disstributions of the different heliostats have been created. In the second phase the procedure to superpose the concentration ratio distributions of different heliostats have been explained. This procedure allows to reproduce the incident radiant power per unit area on the receiver surface for any hour, day and aiming strategy.

### 3.1. Image processing

Fig. 3 shows the schematic of the process described in the following subsections.

#### 3.1.1. Image acquisition

This first phase consists on the characterization of the reflected beam of each heliostat. To do that, a passive screen of 1.4 m length and 1 m height is used. It is located 2.5 m under the cavity and with the same inclination angle. This screen is a solar flux qualification system coated with a white Lambertian paint. The homogeneity of its surface make it ideal to characterize the luminosity of the reflected beam of the heliostats. However, this screen is not refrigerated and only one heliostat can be focused on it at once.

On the ground, in the middle of the solar field, a high resolution CCD camera with adapted filters takes pictures of the beam which is reflected onto the passive screen. The camera is a Theta system SIS1-s28, with a resolution of 2.597 mm per pixel. Besides, the passive target was equipped in its central position with a Vatell flux sensor type TG9000-25, that allows to measure punctual solar flux

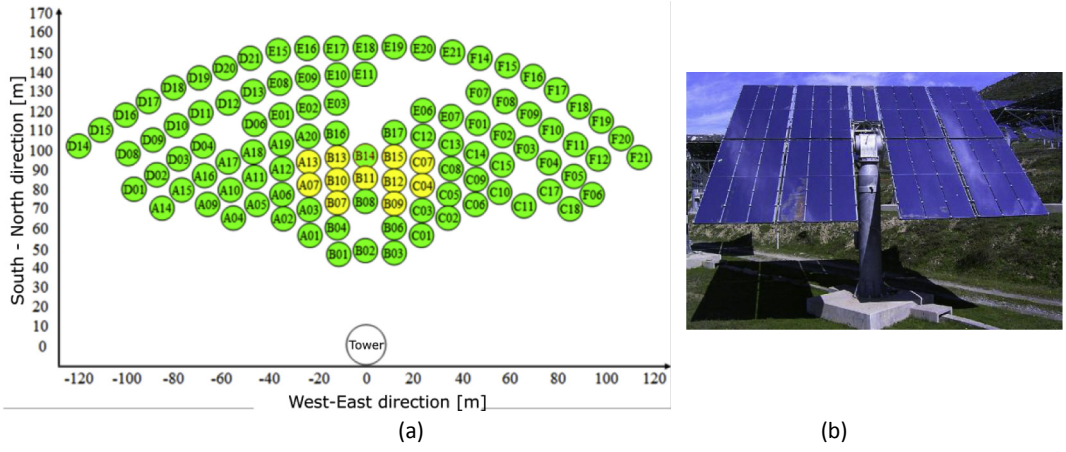


**Fig. 1.** (a) Representation of the heliostat field layout of Themis. (b) Frontal part of a Themis heliostat [31].

intensities. The sensitive sensor consists in a disk of 4.76 mm diameter, equipped of a sapphire window that ensures a pure radiative measurement eliminating convection effects with an accuracy of ±3%. Theoretically, this central point of the screen should correspond to the peak flux of the heliostat beam. The data acquired by the flux sensor is read at the same instant of time in which the picture is taken and the direct normal irradiation (DNI) is acquired. To collect the meteorological data a meteorological station placed at the roof of Themis tower is employed. The station is equipped with a pyrheliometer that measures the DNI every passing minute with a precision of ±1 W/m$^2$.

### 3.1.2. Digital image analysis (DIA)

The raw images taken by the CCD camera are treated with a DIA using the free software "*ImageJ*". This process allows to obtain the luminosity of the reflected beam of the images. For each picture two different surfaces are selected to characterize the average luminosity in the horizontal axis. The raw image of Figs. 4 and 5 represents the reflected beam of heliostat B10 the 30/03/2016 at 11:22 h (civil time).

Firstly, the luminosity has been characterized in the central line of the target (blue solid line in raw image of Fig. 4), which crosses the flux sensor. The luminosity is obtained in grayscale level; whose range goes from 0 to 255. Analysing this central line and not only the central point where the flux sensor is located is mandatory, since the sensor has different reflectivity than the passive screen and then a peak appears in the luminosity signal (yellow point). It is important to note also that there are another atypical values (red points) due to the perforations that the passive screen has every 20 cm, as can be seen in the raw image. These defects in the luminosity have been solved with the average between the closest points (black solid line in Fig. 4). Once the signal has been treated, it is possible to link the flux measurement with a greyscale value (yellow dashed line in Fig. 4).

Secondly, the luminosity has been characterized in a rectangular section of the target (green dashed line in raw image of Fig. 5). This section corresponds to the equivalent area of the high temperature absorber. The average luminosity of that section has been converted to the grayscale level. In this case, the anomalous points still appear, but they are much lower as it corresponds to a lower area in the region scrutinized. Nevertheless, they have been corrected (black solid line) as in Fig. 4. Then, it is possible to use the prior relationship between the grayscale and the flux intensity.

### 3.1.3. Data conversion

In this step it is required to convert the pixels to meters and the grayscale level to flux intensity. For the first transformation, the resolution of the camera has been used. Besides, the position of the flux sensor (maximum peak) has been selected as the origin of coordinates. For the second transformation, a lineal relationship has been assumed between the grayscale level and the flux intensity. The relationship, seen in Fig. 4, has been used to transform the grayscale signal of Fig. 5 to flux intensity, as is plotted in Fig. 6.

The flux intensity depends on the DNI, thus it is preferable to work with concentration ratio, which is defined as the instantaneous flux intensity over the corresponding DNI. Solid green line of Fig. 6 illustrates the concentration ratio distribution on the central area of the target for heliostat B10 at the same day an hour than Figs. 4 and 5. In those figures it can be observed that the grayscale level does not reach the 0 value. The reflected beam spot is larger than the target size, thus heliostat B10 has spillage losses and the concentration distribution obtained from the image is incomplete. An extrapolation at the beginning and end of the signal has been applied to reach the null concentration ratio (solid black line in Fig. 6).

It must be highlighted that the reflected beam is not a perfect ellipse, which reveals some canting and alignment errors of this heliostat. Moreover, the maximum value is slightly displaced to the left with respect to the flux sensor position (x = 0 m), which reflects also a tracking defect of heliostat B10.

### 3.1.4. Library creation

The concentration ratio distribution of each heliostat varies along the year, thus only one picture of each heliostat is not enough to characterize its behaviour. This variation is more pronounced in non-aligned heliostats than in heliostats at perfect conditions. Fig. 7 portrays an example of this variation. It shows several isoflux images, obtained from the raw images [30], of the reflected beam of heliostat B10 along a sunny day. It can be observed that at 10 h the heliostat seems to be on perfect conditions, however at first hours

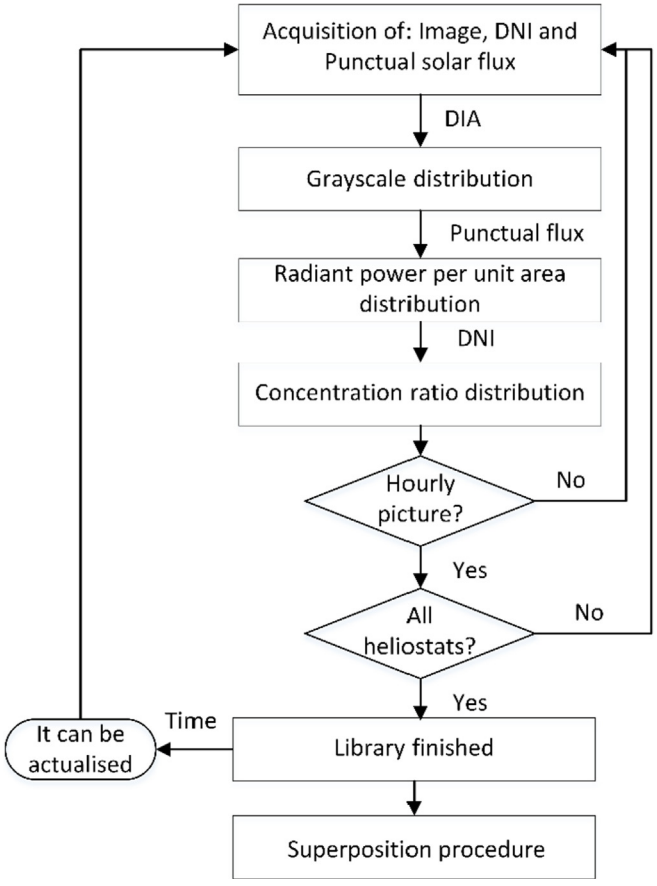


**Fig. 3.** Schematic of the image processing.

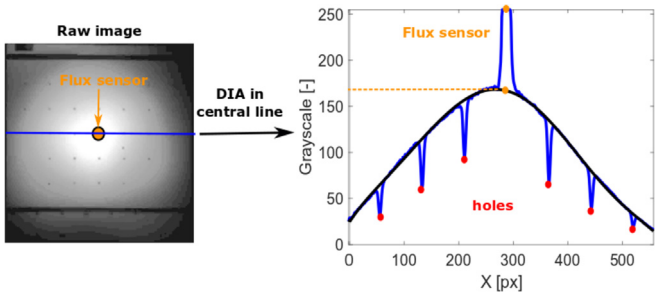


**Fig. 4.** Raw image of the reflected beam of heliostat B10 the 30/03/2016 at 11:22 h. Post-processed information: luminosity in the central line of the target.

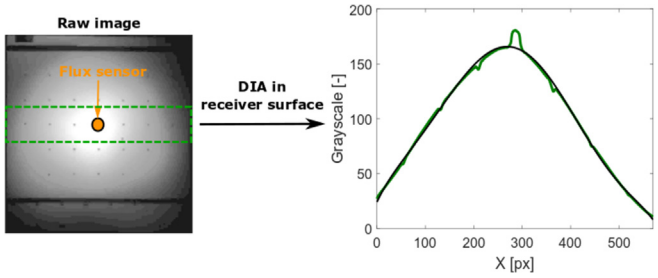


**Fig. 5.** Raw image of the reflected beam of heliostat B10 the 30/03/2016 at 11:22 h. Post-processed information: average luminosity in an area equivalent to the one of the high temperature absorber.

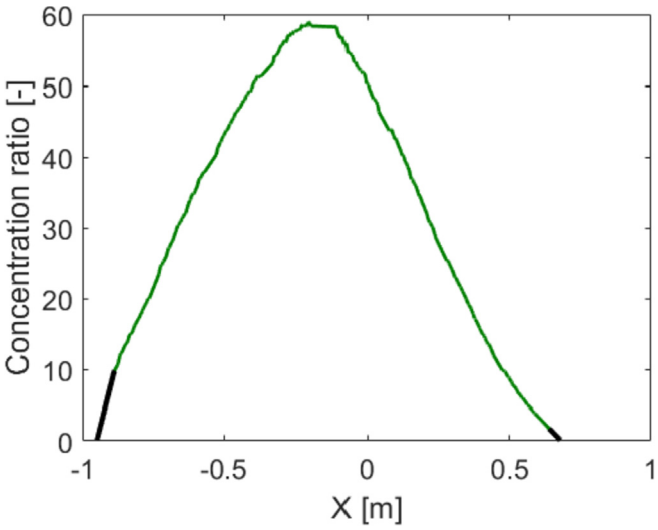


**Fig. 6.** Concentration ratio distribution of the heliostat B10 in the central section of the passive screen the 30/03/2016 at 11:22 h.

in the morning its shape is irregular and in the afternoon there are two focus points (maximums) instead of one.

To solve this problem a library of images of each heliostat has to be created. Fig. 8a represents the concentration ratio distribution of heliostat B10 for two different days at the same solar hour, while Fig. 8b depicts the concentration ratio distribution of the same heliostat at different hours of a sunny day. In Fig. 8 it can be seen that the annual concentration ratio distribution remains almost constant when the solar hour is fixed, however it varies considerably with the time variation. Therefore, it can be assumed that the library is independent on the day but not on the solar hour.

To complete the library is recommendable to have more than one image per hour of each heliostat. It permits to do reliable weighted averages between several concentration ratio distributions of a heliostat to obtain its approximate behaviour at any time. Besides, it is recommendable to take these photos at different days along the year to reduce the errors in the characterization of the heliostat, as it minimises the effect of the reflectivity variation caused by the weather conditions or the cleaning of the heliostat.

### 3.2. Superposition procedure

In the second phase the average concentration ratio distribution of the individual heliostats has to be gathered in order to obtain the incident thermal power on the receiver.

Firstly, the solar hour of the analysis has to be fixed, since it is required to obtain the most adequate concentration ratio distributions from the library. For each heliostat a weighted average between concentration ratio distributions closer in time has to be done, the resultant of this operation is used in the next steps. Based on the amount of data available three images, for each heliostat, were chosen enough to minimise the uncertainties due to time gap, atmospheric conditions and season (day of the year) with a reasonable increment of the computational cost. However, the number of averaged images could be reduced if not enough data are available or increased if there are too many available pictures close to the hour of study.

Secondly, the aiming strategy has to be selected. In the prototype receiver, 11 heliostats aimed to 7 different points in the same horizontal line, as shown in Fig. 9. The origin of coordinates corresponds to the central position of the high temperature absorber. Therefore, the resultant concentration ratio of each heliostat has to be displaced in the horizontal position the corresponding distance given by Fig. 9. As the passive screen and the high temperature absorber are relatively close, the variations on the reflected beam when the heliostats aim to the target or to the high temperature absorber can be neglected. Pacheco et al. [28] examined the effect of focus variation due to spatial shift and time gap during experiments carried out in an external receiver. They determined that this error is greater for heliostats in the rows closer to the tower and

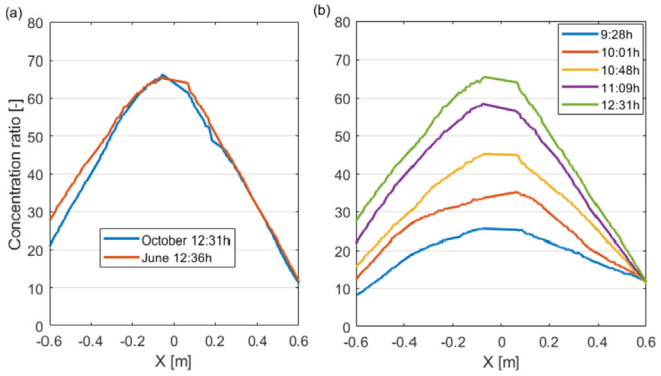


**Fig. 8.** Distribution of the average concentration ratio for heliostat B10 at (a) two different days at the same hour, and at (b) the same day at different hours.

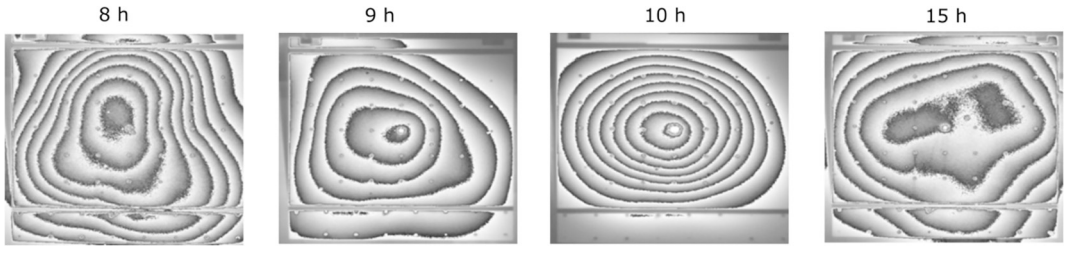


**Fig. 7.** Isoflux images of the reflected beam of heliostat B10 at different hours of a sunny day.

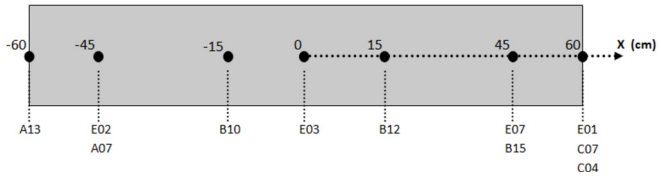


**Fig. 9.** Aiming strategy used on the solar receiver prototype.

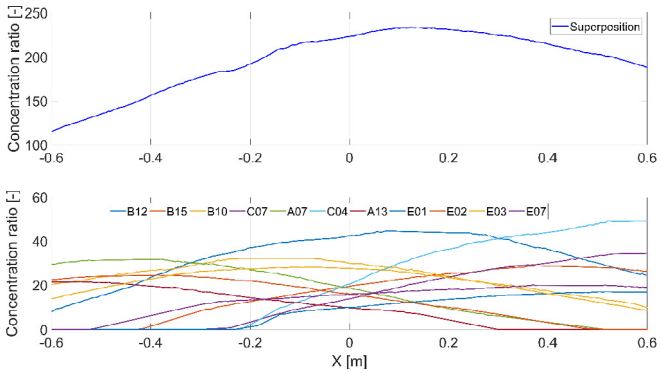


**Fig. 10.** Resultant concentration ratio of the 11 heliostats focused to different horizontal positions (see Fig. 9). Bottom: Individual concentration ratio distributions. Top: Superposed concentration ratio distribution.

lower for the heliostats at the edges. This error increases with the separation between the receiver and the target and the modification of the interception plane. However, they pointed that this error is relatively small (around 2%) compared to other errors as: variation of the atmospheric conditions, camera linearity and variations in the white target properties.

Fig. 10 (bottom) represents the resultant concentration ratio of each individual heliostat once the aiming strategy has been applied. The horizontal axis represents the length of the high temperature absorber (1.2 m). It can be observed that the selected aiming strategy has important spillage losses, especially in the inlet of the absorber (right side). Fig. 10 (top) portrays the sum of the individual concentration ratio presented in Fig. 10 (bottom). The incident solar flux on the high temperature absorber is calculated multiplying the total concentration ratio by the instantaneous DNI at the desired moment.

## 4. Verification of the method

To verify the main assumptions made in Superposition method a set of experiments were carried out after dismantling the high temperature absorber. A rigid insulation panel of compacted $Al_2O_3$ fibbers 1 m × 0.2 m x 0.05 m has been assembled in the absorber position. As it has a homogeneous colour, it can be used as a passive target in the back of the cavity. A Vatell flux sensor was installed in the center of the insulation panel to measure the punctual incident flux, see Fig. 11.

Images of the back of the cavity were taken with the CCD camera when different number of heliostats were focused on the insulation panel. Independently on the number of heliostats used, each working heliostat focus to its respective point indicated in Fig. 9. To the raw images of the reflected beams on the insulation panel the same DIA than in the passive screen images has been applied. In this case, the grayscale level takes into account the effect (shadows) of the cavity lateral walls.

In Fig. 12 the incident flux distributions obtained in the insulation panel, when 4, 8 and 11 heliostats were focused to the back of

**Fig. 11.** Assemble of the rigid insulation panel with the flux sensor in the middle.

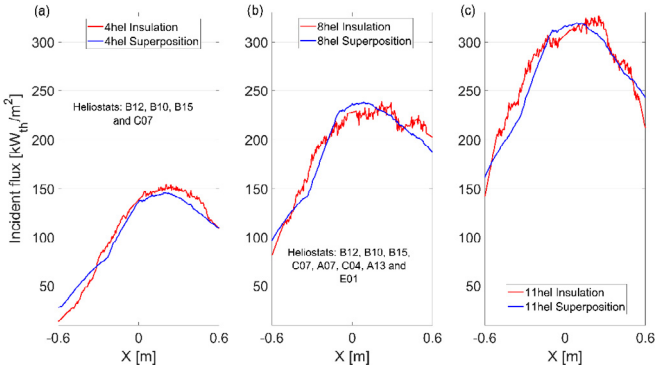


**Fig. 12.** Comparison between the solar flux distribution on the insulation panel and the calculated by Superposition on the central section of the high temperature absorber for the day 19/07/2016, using (a) 4 heliostats at 14:59 h (b) 8 heliostats at 15:19 h (b) 11 heliostats at 15:44 h.

the cavity, have been compared with the results of the Superposition method at the same hour. It is observed that with the three aiming strategies the solar flux distribution obtained in the insulation panel agrees well with the method proposed. The radiant power per unit area is slightly underestimated with the Superposition method (about 2.5%) and the differences are constant with the number of heliostats focused. These small differences can be attributed to: the effect of the lateral walls of the cavity, which is only considered in the insulation panel; the variation of the aiming position (passive screen or back of the cavity), and a possible wrong estimation of the averaged reflected beam of the individual heliostats due to the lack of information on the library at certain hours.

Due to the technical difficulty of the plant operation further verifications were not possible. With the available data it can be pointed that, despite the approximations made, Superposition method is able to obtain a good approximation of the solar flux distribution and intensity that falls upon the high temperature absorber. Moreover, it has been tested that Superposition method can be adapted easily to different aiming strategies and hours since the heliostats have been individually characterized.

### 4.1. Uncertainty considerations

The uncertainty of the proposed Superposition method depends on:

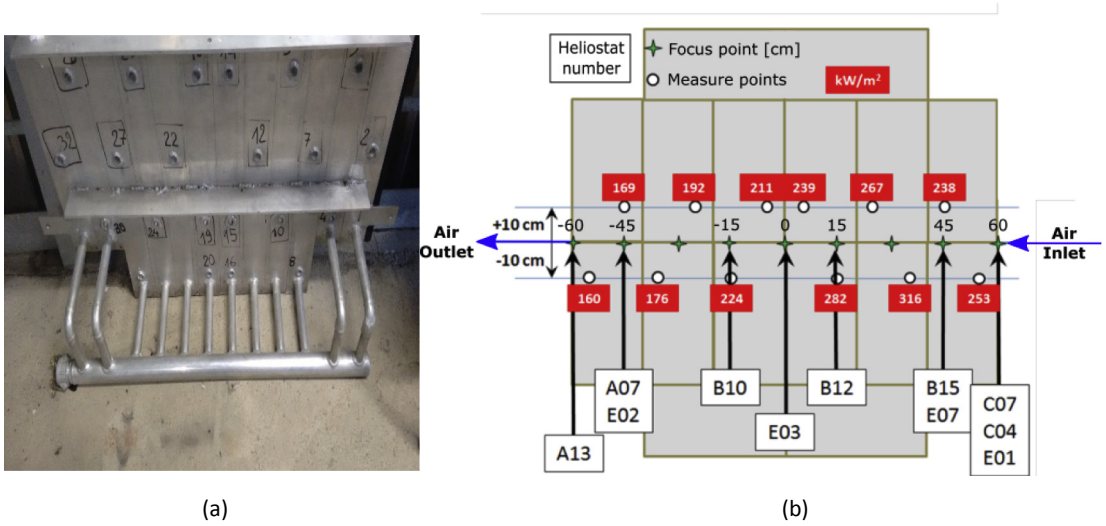


**Fig. 13.** (a) Image of the dismantled cooled panel (b) Schematic of the cooled panel including the focus point of the 11 heliostats (white rectangles and green crosses) and the intensity of each of the 12 solar flux (red rectangles and white points) for the 07/01/2015 at 16:11 h (civil time).

- The accuracy of heliostat tracking: which treats to be corrected using the white target before focusing the heliostats to the receiver.
- The number of heliostats involved in the test: although in previous subsection it has seen that the accuracy is independent of the heliostat number.
- The time gap between the heliostat characterization and the tests on the receiver: this effect has been corrected with the library creation and the solar flux distribution average.
- Variation of the atmospheric conditions and mirrors cleanliness: this effect is also minimised averaging solar flux distributions of each heliostat.
- The spatial shift between the white screen and the receiver and effect of the lateral walls of the cavity: comparing two consecutive images (time gap lower than a minute) of the reflected beam of heliostat B12 on the white screen and on the insulation panel, the differences find between both flux distributions is 2.7%.
- Uncertainties of CCD camera and the flux sensor that can be assumed around 3%,
- Painting deterioration of the target an insulation panel: The target is frequently cleaned and the insulation panel was used during a few number of experiments to avoid that problems.

Therefore, the error of the proposed method is similar to the one obtained by Pacheco et al. [28] being lower than 10%, which is acceptable for experimental results.

## 5. Validation

In this section the Superposition method has been validated using flux measurements carried out in the back of the cavity before installing the receiver prototype. A metallic cooled panel was assembled in the back wall of the cavity (Fig. 13a); it possesses 32 holes distributed by its entire surface, but only 12 of which are sited on the high temperature absorber location. In these 12 holes, different Vatell cooled flux sensors were installed.

Fig. 13b schematizes the cooled panel and portrays the aiming strategy described in Fig. 9. Besides, the intensity of the solar flux measured in each of the 12 holes for the 7th of January of 2015 at 16:11 h (civil time) have been shown in the red rectangles. These 12 measures give the distribution of incident radiant power per unit area on the high temperature absorber surface (red circles in Fig. 14).

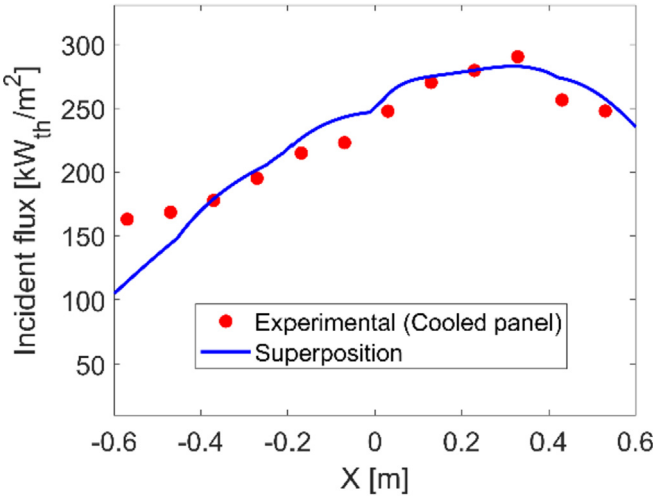


**Fig. 14.** Comparison between the incident solar flux measured in the cooled panel and the calculated by the Superposition method the 07/01/2015 at 16:11 h.

Fig. 14 displays the solar flux distribution and intensity on the high temperature absorber position, during the 7th of January of 2015 at 14:19 h solar time (16:11 h civil time) measured in the cooled panel and calculated using Superposition method. The distribution of radiant power per unit area is similar in both cases. Therefore, the assumption of proportionality between the grayscale level and the flux intensity is correct.

Integrating both signals it is obtained a total solar flux on the equivalent receiver surface of 253 $kW_{th}/m^2$ for the measurement in the cooled panel and 276.27 $kW_{th}/m^2$ for the Superposition method, which represents a variation of 8.4%. This variation is slightly higher than the obtained in the uncertainty analysis, due to none location of the 12 measurement points are located in the middle height of the receiver, where the flux is expected to be the highest, and thus the cooled panel underestimates the incident flux intensity on the receiver. At the inlet and exit of the high temperature absorber the differences between both signals increase. The

flux measured on the cooled panel presents slope variations close to the edges due to the radiative heat exchange with the lateral walls of the cavity; effect that is not considered in the Superposition method. Overall it can be concluded that the Superposition method constitutes a good approximation for the flux density calculation.

## 6. Conclusions

In this study, a new empirical direct methodology named "*Superposition method*" has been developed to determine the distribution and intensity of the solar flux that falls upon a central receiver surface. The methodology is especially useful when the heliostats are deteriorated and the numerical simulations are not able to predict the incident solar flux. This methodology has been verified and validated on a high temperature absorber installed in the back of a cavity on Themis solar power tower, whose heliostats are far from the nominal conditions.

"*Superposition method*" characterizes separately each heliostat to gather the individual flux distributions using digital image analysis. The method requires creating an hourly library to characterize each heliostat. Once the library is well defined it is a non-real-time method that allows to predict the solar flux distribution and intensity on the high temperature absorber at any moment with minimum grade of error. Characterizing the heliostats individually permits to test different aiming strategies without excessive effort. Besides, to minimising the error the authors encourage to extend the library always that it was possible, to adapt it to the new conditions of the heliostats.

The strength of the proposed experimental methodology compared to others of the literature is the time independence that allows to estimate solar flux distributions without carrying out extra measurements, the good spatial resolution and the low cost. However, the main issue related to Superposition methodology is the time cost of creating the proposed library for large solar fields. As the heliostats are characterized individually, the heliostats could be defocused of the receiver during operation without perturbing the solar plant operation, being the available time the only problem of the proposed methodology for its implantation in commercial power plants. Nonetheless, it is useful in demonstration solar power towers as Themis or to characterize those heliostats, inside large solar fields, that may present calibration or geometrical problems.

Moreover, the creation of the library can be a good starting point to develop further strategies to control problematic heliostats and to introduce the heliostat deterioration parameters in numerical models.

## Acknowledgments

The authors acknowledge the financial support of the research programme of the University Carlos III de Madrid, which made this study possible through a mobility grant of the first author. Moreover, the research work leading to this article received funding from the European Union Seventh Framework Program (FP7/2014-2018) under grant agreement no. 609837 (Scientific and Technological Alliance for Guaranteeing the European Excellence in Concentrating Solar Thermal Energy, STAGE-STE). This work was also supported by the Spanish government under the project ENE2015-69486-R (MINECO/FEDER, UE).

## References

[1] European energy research alliance, STAGE-STE project [WWW Document], 2014. http://www.stage-ste.eu/. http://www.stage-ste.eu/ (accessed 4.4.2016).

[2] N.C. Cruz, J.L. Redondo, M. Berenguel, J.D. Álvarez, P.M. Ortigosa, Review of software for optical analyzing and optimizing heliostat fields, Renew. Sustain. Energy Rev. 72 (2017b) 1001–1018. https://doi.org/10.1016/J.RSER.2017.01.032.

[3] P. Garcia, A. Ferriere, J.-J. Bezian, Codes for solar flux calculation dedicated to central receiver system applications: a comparative review, Sol. Energy 82 (2008) 189–197. https://doi.org/10.1016/j.solener.2007.08.004.

[4] P.L. Leary, J.D. Hankins, User's Guide for MIRVAL: a Computer Code for Comparing Designs of Heliostat-receiver Optics for Central Receiver Solar Power Plants, 1979.

[5] T. Wendelin, SolTRACE: a new optical modeling tool for concentrating solar optics, Sol. Energy (2003) 253–260. https://doi.org/10.1115/ISEC2003-44090.

[6] M.J. Blanco, J.M. Amieva, A. Mancilla, The tonatiuh software development project: an open source approach to the simulation of solar concentrating systems, in: ASME International Mechanical Engineering Congress and Exposition. Orlando, Florida, USA, 2005, pp. 1–8.

[7] B. Belhomme, R. Pitz-Paal, P. Schwarzbözl, S. Ulmer, A new fast ray tracing tool for high-precision simulation of heliostat fields, J. Sol. Energy Eng. 131 (2009) 31002. https://doi.org/10.1115/1.3139139.

[8] J.P. Roccia, B. Piaud, C. Coustet, C. Caliot, E. Guillot, G. Flamant, J. Delatorre, SOLFAST, a ray-tracing monte-carlo software for solar concentrating facilities, J. Phys. Conf. Ser. 369 (2012). https://doi.org/10.1088/1742-6596/369/1/012029.

[9] P. Schwarzbözl, R. Pitz-Paal, M. Schmitz, Visual HFLCAL - a software tool for layout and optimisation of heliostat fields, in: SolarPACES. SolarPACES, Berlin, Germany, 2009.

[10] B.L. Kistler, A User's Manual for DELSOL3: a Computer Code for Calculating the Optical Performance and Optimal System Design for Solar Thermal Central Receiver Plants. Albuquerque, 1986.

[11] F.J. Collado, One-point fitting of the flux density produced by a heliostat, Sol. Energy 84 (2010) 673–684. https://doi.org/10.1016/j.solener.2010.01.019.

[12] F.J. Collado, J. Guallar, Campo: generation of regular heliostat fields, Renew. Energy 46 (2012) 49–59. https://doi.org/10.1016/j.renene.2012.03.011.

[13] A. Sánchez-González, D. Santana, Solar flux distribution on central receivers: a projection method from analytic function, Renew. Energy 74 (2015) 576–587.

[14] P. Piroozmand, M. Boroushaki, A computational method for optimal design of the multi-tower heliostat field considering heliostats interactions, Energy 106 (2016) 240–252. https://doi.org/10.1016/J.ENERGY.2016.03.049.

[15] N.C. Cruz, J.L. Redondo, M. Berenguel, J.D. Álvarez, A. Becerra-Teron, P.M. Ortigosa, High performance computing for the heliostat field layout evaluation, J. Supercomput. 73 (2017a) 259–276. https://doi.org/10.1007/s11227-016-1698-7.

[16] M.R. Rodríguez-Sánchez, A. Sánchez-González, D. Santana, Revised receiver efficiency of molten-salt power towers, Renew. Sustain. Energy Rev. 52 (2015) 1331–1339. https://doi.org/10.1016/j.rser.2015.08.004.

[17] J. Fernández-Reche, Reflectance measurement in solar tower heliostats fields, Sol. Energy 80 (2006) 779–786. https://doi.org/10.1016/J.SOLENER.2005.06.006.

[18] M. Chiesi, E.F. Scarselli, R. Guerrieri, Run-time detection and correction of heliostat tracking errors, Renew. Energy 105 (2017) 702–711. https://doi.org/10.1016/J.RENENE.2016.12.093.

[19] X. Wei, Z. Lu, W. Yu, H. Zhang, Z. Wang, Tracking and ray tracing equations for the target-aligned heliostat for solar tower power plants, Renew. Energy 36 (2011) 2687–2693. https://doi.org/10.1016/j.renene.2011.02.022.

[20] A. Sánchez-González, C. Caliot, A. Ferrière, D. Santana, Determination of heliostat canting errors via deterministic optimization, Sol. Energy 150 (2017) 136–146. https://doi.org/10.1016/j.solener.2017.04.039.

[21] M. Röger, P. Herrmann, S. Ulmer, M. Ebert, C. Prahl, F. Göhring, Techniques to measure solar flux density distribution on large-scale receivers, J. Sol. Energy Eng. 136 (2014) 31013. https://doi.org/10.1115/1.4027261.

[22] J. Strachan, R. Houser, Testing and Evaluation of Large-area Heliostats for Solar Thermal Applications, Solar Thermal Test Department, Sandia National Laboratories, Albuquerque, 1993. SAND92–1381.

[23] G. Vontobel, C. Schelders, M. Real, Concentrated Solar-flux Measurements at the IEA-ssps Solar-central-receiver Power Plant, Tabernas - Almeria (Spain). Wuerenlingen (Switzerland), 1982.

[24] A. Kroger-Vodde, A. Hollander, CCD flux measurement system PROHERMES, J. Phys. IV Fr. 9 (1999) 649–654.

[25] A. Imenes, J. Hinkley, R. Benito, R. Bolling, P. Schramek, S. Ulmer, Ray tracing and flux mapping as a design and research tool at the national solar energy centre, in: ANZSES Conference. Canberra, 2006, pp. S06–S81.

[26] J. Ballestrín, R. Monterreal, Hybrid heat flux measurement system for solar central receiver evaluation, Energy 29 (2004) 915–924. https://doi.org/10.1016/S0360-5442(03)00196-8.

[27] C.K. Ho, S.S. Khalsa, A photographic flux mapping method for concentrating solar collectors and receivers, J. Sol. Energy Eng. 134 (2012) 41004. https://doi.org/10.1115/1.4006892.

[28] J.E. Pacheco, R.M. Houser, A. Neumann, Concepts to measure flux and temperature for external central receivers.pdf, in: Joint Solar Engineering Conference, 1994, pp. 595–603.

[29] J.E. Pacheco, Final Test and Evaluation Results from the Solar Two Project. Albuquerque, 2002. SAND2002–0120.

[30] A. Salomé, F. Chhel, G. Flamant, A. Ferrière, F. Thiery, Control of the flux distribution on a solar tower receiver using an optimized aiming point strategy: application to THEMIS solar tower, Sol. Energy 94 (2013) 352–366. https://

doi.org/10.1016/j.solener.2013.02.025.
[31] A. Salomé, G. Flamant, A. Ferrière, F. Thiery, Optimized Aim Point Strategy for Central Receiver : Application to Themis, SolarPACES, 2012.
[32] CNRS-PROMES, PROMES Facilities: Themis [WWW Document], 2013. http://www.promes.cnrs.fr/index.php?page=themis (accessed 2.25.2018).
[33] J. Capeillère, a. Toutant, G. Olalde, A. Boubault, Thermomechanical behavior of a plate ceramic solar receiver irradiated by concentrated sunlight, Sol. Energy 110 (2014) 174–187. https://doi.org/10.1016/j.solener.2014.08.039.